PHYSICSAccess Research Paper
ISSN Online: 2756-3898, ISSN Print: 2714-500X https://doi.org/10.47514/phyaccess.2024.4.1.008

Investigating the influence of precursor temperature on the bandgap energy, structural, and morphological features of Ti-doped barium sulphide material for photovoltaic application

Emmanuel O Okechukwua[1], Imosobomeh L Ikhioya[2] and Azubuike J Ekpunobi[1]

[1] Department of Physics and Industrial Physics, Nnamdi Azikiwe University, Awka, Anambra State, Nigeria
[2] Department of Physics and Astronomy, University of Nigeria, Nsukka, 410001, Enugu State, Nigeria

Corresponding E-mail: imosobomeh.ikhioya@unn.edu.ng

Received 28-05-2024
Accepted for publication 11-06-2024
Published 13-06-2024

Abstract

In this study, we use electrochemical deposition on FTO to grow BaTiS thin films. By varying the temperature of the precursors, we conducted thorough growth studies to understand how these process parameters affected the structure of BaTiS films. The diffraction peaks in the XRD pattern match the cubic barium sulfide structural phase. The observed peaks, 39.994 ° and 65.742 ° at 35 °C; 39.982 ° and 65.717 ° at 45 °C, and 39.995 °, 63.920 °, and 65.856 ° at 55 °C. The film deposited at 55 °C had a surface morphology with uniformly distributed spherical-shaped particles that formed agglomerations. The film's surface was smooth, providing a clearer look at the grain boundaries, suggesting a polycrystalline composition. The films deposited at temperatures of 35 °C, 40 °C, 45 °C, 50 °C, and 55 °C yielded energy band gaps of 2.98 eV, 2.90 eV, 2.69 eV, 2.68 eV, and 2.30 eV, respectively. The result showed that the films' energy band gap decreased as the deposition temperature increased. The varied energy bandgap of the films confirmed the effects of deposition temperature on the films.

Keywords: BaTiS; bandgap energy; structural; morphology; Metals; FTO.

I. INTRODUCTION

The world has become a "global village" due to the transformation brought by ICT. Without a doubt, the progress of semiconductors has fueled technological development, and our lives now revolve around this technology [1]–[12], [13]. Electronics have played a significant role in shaping modern society. Semiconductors, especially silicon, are crucial elements in most electronic devices [14]. The rise in science and technology has led to a growing need for smaller, more affordable, and faster memory devices for specific purposes [15]–[19]. In the automobile, telecommunication, and electronic gadget industries, these devices have diverse applications. Spintronics technology offers the potential for more affordable, smaller, and quicker electronic devices [20]. Initially, the spintronics program focused on supervising the advancement of spin transport electronics for magnetic memory and sensors. The expansion of the project included SPINS, aiming to revolutionize semiconductor electronics using electron spin freedom. Technology advancements dominate in portable memory. Spintronics is one of the portable solutions that offer vast

space, small size, and fast response in response to the rapid growth in technology. Using electron charge and spin to carry information in technology has great potential for fulfilling memory requirements of large space, small size, and fast response in various applications. Adding spin freedom to electronic devices could offer advantages [21], such as non-volatility, faster data processing, lower power consumption, and increased integration densities.

Magneto-optical devices, microelectronics, and diodes frequently employ barium chalcogenides [22]–[30]. Different techniques can deposit thin films of barium sulfide, a chalcogenide, synthesized by various methods [31]–[38]. BaS is unique compared to other alkaline-earth chalcogenides because of its exceptional ionic features and metallization properties at high pressures. Therefore, BaS finds applications in different optoelectronic devices. BaS is an essential compound for producing a range of barium-based substances used in ceramics, flame inhibitors, dyes, and additives. [39], [40]. In the present era, optoelectronic devices are becoming increasingly important. BaS stands out among other barium chalcogenides due to its remarkable ratio of cations and anions [39], [41], [42]. The presence of oxygen makes barium sulphide unstable, but with controlled preparation and usage, it can yield improved outcomes.

Reference [42] employed the Chemical Bath Deposition Technique for depositing Barium Sulphide semiconductor thin films on a glass substrate. The films show low absorbance and reflectance, ranging from 0.002 to 0.065. The films exhibited a high level of transparency to the incident radiation, ranging from 0.950 to 0.993. The films showed a wide range of optical conductivity, from 7.43×10^{10} S^{-1} to 5.52×10^{12} S^{-1}, with thicker films observed as the dip time increased from 1.668 to 1.775 µm. The measured band gap energy of the deposited films falls within the range of 1.25 to 1.35. The semiconductor material's desirable traits made it perfect for developing photonics and photovoltaic devices. Reference [41] examined the impact of film thickness on the transmittance of barium sulphide thin film deposited by the chemical bath. Films of different thicknesses applied to glass substrates by dipping for different durations: 12, 24, 36, and 48hrs. The results indicated that the films have a high transmittance level between 0.989 and 0.991. The film that has the highest thickness, approximately t = 2.360µm, shows a transmittance of 0.991. The film, which is about 2.212µm thick, has a transmittance of 0.968. The longer the dip time, the thicker the film became.

Through electrochemical deposition, we achieve the growth of BaTiS thin films on FTO substrates in this study. Our thorough growth studies on the BaTiS material involved varying precursor temperatures to investigate its impact on bandgap energy, structure, and morphology of the synthesized films. High-resolution X-ray diffraction and scanning electron microscopy were used to study the structure and surface of the as-grown films.

II. METHODS

The electrochemical deposition technique requires the use of three electrodes for film deposition. The electrodes were connected to a D.C power supply device. These electrodes were placed inside a container containing a liquid (an electrolyte) which has ionic species dissolved within it. The electrolytes, power supply unit, and electrodes make up the electrodeposition setup. The setup involves three electrodes and is designed for depositing thin films on conducting substrates. In this work, the conducting substrates (FTO) were used as the working electrode, which is the cathode; the graphite rod was used as the counter electrode, which is the anode; and the silver/silver chloride electrode (Ag/AgCl) was used as the reference electrode, and they are connected to a source of energy supply.

A. Deposition of Barium Sulfide (BaS) Thin Film

The bath solution for the deposition of BaS thin film contained 15 ml of 0.05 molar concentration of barium acetate ($C_4H_6BaO_4$) as a source barium ion (Ba^{2+}) and 15 ml of 0.050 molar concentration of thiourea ($CH4N_2S$) as a source of sulfur ion (S^{2-}). The solution was mixed properly using a magnetic stirrer. The 0.05 M of barium acetate ($C_4H_6BaO_4$) was measured by dissolving 6.4 g of it in 500 ml of distilled water, and the 0.050 M of CH_4N_2S was measured by dissolving 1.9 g of it in 500 ml of distilled water. The film deposition took place at room temperature of 27 °C. The pH value (5.6) of the bath solution was obtained using a pH meter. The deposition time and voltage were kept at 120 s and 5 V respectively. After deposition, the substrate containing the deposited film was taken out of the solution and immersed in distilled water for just two seconds to remove any unwanted particles from the surface of the substrate and then dried up in flowing air. Afterwards, the samples were placed in a slide box, and labeled accordingly.

B. Variation of Bath Temperature for BaTiS Thin Films Deposition

Keeping every other parameter constant, heating varied the solution bath (precursors) temperature, using a hotplate. A laboratory thermometer was used to monitor the temperature. The film deposition took place at a temperature range of 35– 55 ℃ at an interval of 5 ℃, voltage value of 7.5 V, and time of 90 s.

III. RESULT AND DISCUSSIONS

A. Effect of temperature variation on the structural properties of Ti-doped barium sulfide films

Fig. 1 depicts the XRD patterns of titanium-doped barium sulfide films deposited at different bath temperatures. The diffraction patterns in XRD correspond to the cubic barium sulfide structural phase. The observed peaks, 39.994 ° and 65.742 ° at 35 °C; 39.982 ° and 65.717 ° at 45 °C, and 39.995 °, 63.920 °, and 65.856 ° at 55 °C correspond to the peaks in the standard Powder Diffraction File (PDF) card number 01 -

075 - 0896 of JCPDS–ICDD (The Joint Committee on Powder Diffraction Standard - International Centre for Diffraction Data). Peaks corresponding to tin (II) oxide with JCPDS–ICDD file number 00-041-1445 were observed at 26.580 °, 33.796 °, 37.847 °, and 51.636 ° for the film synthesized at 35 °C; 26.566 °, 33.775 °, 37.825 °, and 51.614 ° for the film deposited at a temperature 45 °C, and 26.594 °, 33.811 °, 37.909 °, and 51.688 ° for the film deposited at a temperature 55 °C. The substrate, fluorine-doped tin oxide, is responsible for the presence of tin (II) oxide. The diffraction spectra in Table 1 showed an increase in intensity and a slight shift towards higher angles. The structural parameters of the deposited thin films are shown in Table I.

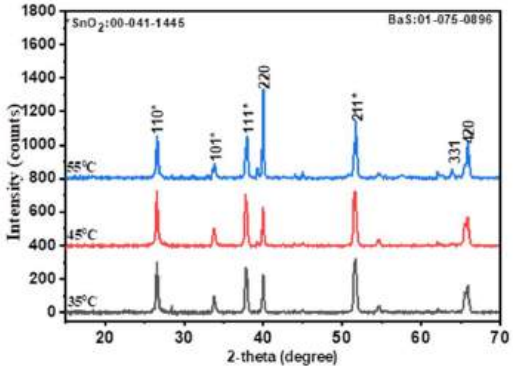

Fig. 1 Structural patterns of Ti-doped barium sulphide thin films at different bath temperatures.

Table I. Structural parameters of Ti-doped barium sulfide thin films at different temperatures.

Materials	2 θ (◦)	hkl	D spacing (nm)	FWHM (◦)	D (nm)	δ x 10^{15} (lines-m^2)	ε x 10^{-3}
35 °C	26.580	110*	3.351	0.290	29.360	1.160	5.364
	33.796	101*	2.650	0.338	25.621	1.523	4.861
	37.847	111*	2.375	0.364	24.087	1.724	4.635
	39.994	220	2.253	0.243	36.272	0.760	2.919
	51.636	211*	1.769	0.396	23.289	1.844	3.570
	65.742	420	1.419	0.635	15.560	4.130	4.287
	Average				25.698	1.857	4.273
45 °C	26.566	110*	3.353	0.291	29.288	1.166	5.380
	33.775	101*	2.652	0.372	23.318	1.839	5.345
	37.825	111*	2.377	0.373	23.533	1.806	4.746
	39.982	220	2.253	0.244	36.116	0.767	2.932
	51.614	211*	1.769	0.304	30.269	1.091	2.747
	65.717	420	1.420	0.518	19.082	2.746	3.497
	Average				26.934	1.569	4.108
55 °C	26.594	110*	3.349	0.300	28.453	1.235	5.532
	33.811	101*	2.649	0.365	23.770	1.770	5.238
	37.909	111*	2.372	0.388	22.609	1.956	4.930
	39.995	220	2.252	0.216	40.884	0.598	2.589
	51.688	211*	1.767	0.401	22.975	1.895	3.615
	63.92	331	1.455	0.328	29.841	1.123	2.292
	65.856	420	1.417	0.345	28.667	1.217	2.323
	Average				28.171	1.430	4.033

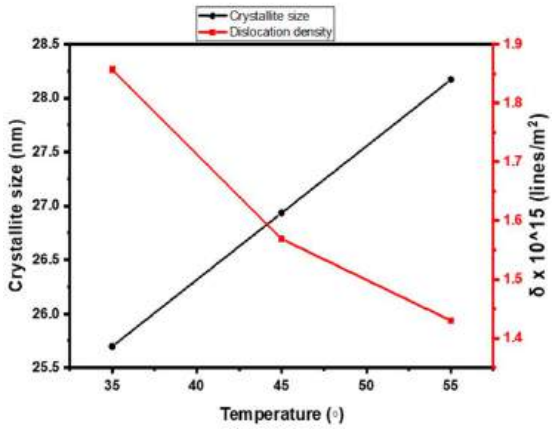

Fig. 2 Plot of crystallite size and dislocation density with temperature for Ti-doped barium sulphide thin film.

The films have crystallite sizes ranging from 25.698 to 28.171 nm on average. The films exhibited an increase in crystallite size and a decrease in dislocation densities and micro-strains, as deposition temperature increases. The findings revealed that increasing the deposition temperature had a positive effect on the crystal structure of the Ti-doped barium sulfide thin films. The observed heightened intensity and sharper peaks in the film deposited at 55 °C provide support for this [13], [14], [19]. Fig. 2 depicts the crystallite size and dislocation density with bath temperature.

B. Effect of temperature on the surface morphology of titanium-doped barium sulfide films

SEM images of titanium-doped barium sulfide films at bath temperatures of 35, 45, and 55 °C are depicted in Fig. 3. Physical observation of the images showed that the film deposited at a temperature value of 35 °C contained a small

amount of grains that were tightly combined. As the deposition temperature was increased to 45 °C, the surface of the film became smooth, indicating a polycrystalline structure. The surface morphology of the film deposited at 55 °C showed an agglomeration of tiny spherical-shaped particles that were uniformly distributed on the surface of the substrate. The surface of the film was flat, with a clearer view of the grain boundaries, indicating a polycrystalline structure.

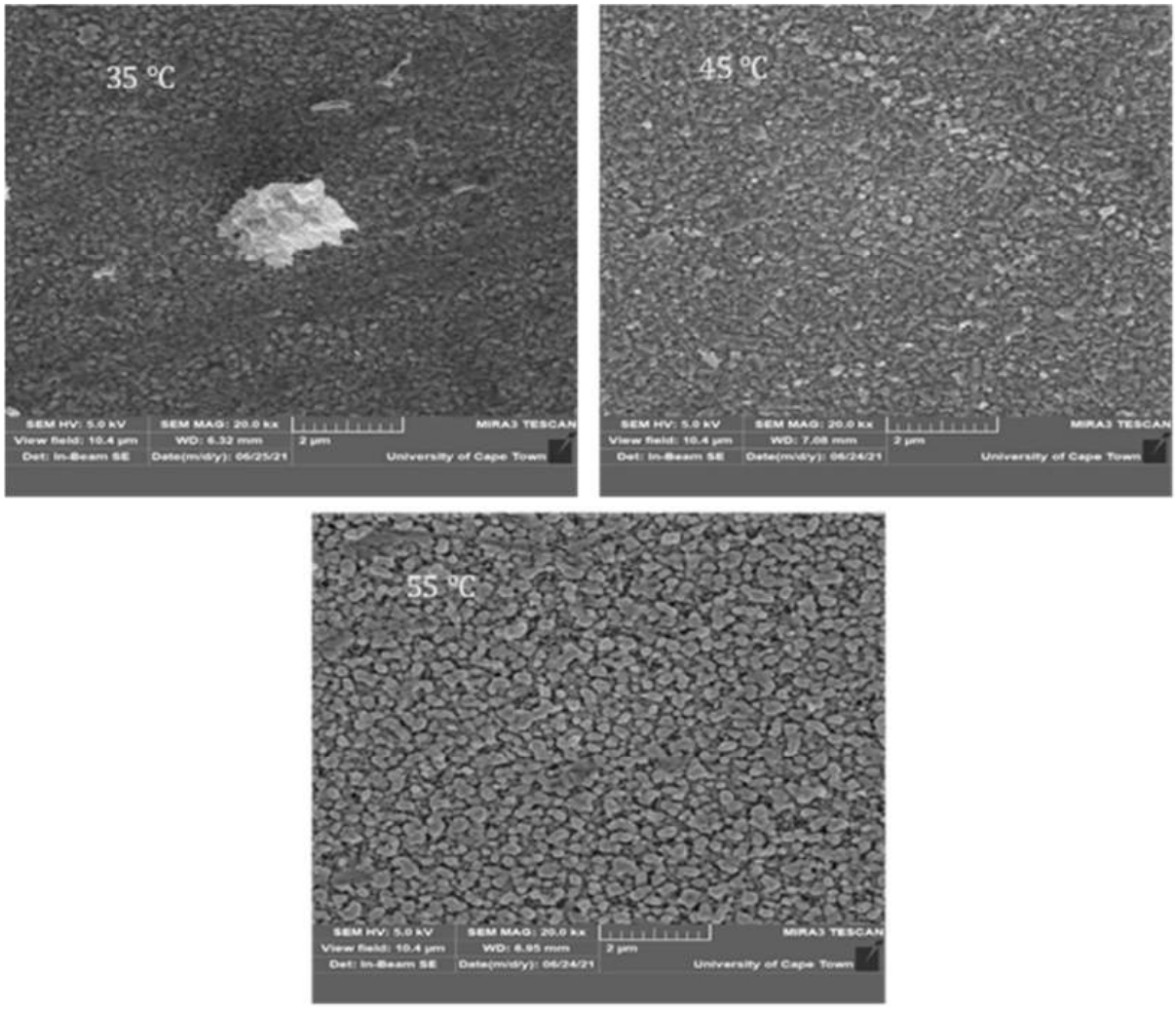

Fig. 3 Micrograph of titanium-doped barium sulphide thin films at different deposition temperatures.

C. Effect of titanium dopant on the elemental composition of barium sulfide films

EDS graphs of electro-deposited undoped and titanium-doped barium sulfide thin films were shown in Fig. 4(a) and (b), respectively. The EDX spectra depicted the atomic weight of the elements present in the deposited thin films. Fig. 4 (a) contained Barium (Ba): 57.09%, Sulphur (S): 23.31%, Silicon (Si): 14.00%, and Calcium (Ca): 5.60%, Fig. 4 (b) contained Barium (Ba): 53.09%, Sulphur (S): 23.00%, Silicon (Si): 13.00%, Calcium (Ca): 7.60%, and Titanium (Ti): 3.31%. The presence of silicon and calcium could result from the composition of the glass substrate. However, the results confirmed the expected elements (Ba, S, and Ti) in the deposited films. Also, physical observation showed that incorporating titanium ions into the structure of barium sulfide reduced the atomic percentage of copper in the deposited films, which was evidence that there was a substitution of barium ion by titanium ion. Fig. 4 (c) shows the EDS graph of Ti-doped BaS thin film, synthesized at a temperature of 35 °C. Along with the EDS spectra, the atomic weight of the elements present in the deposited thin film was presented. The film contained Barium (Ba): 53.39%, Sulphur (S): 23.00%, Silicon (Si): 13.00%, Calcium (Ca): 7.60%, and Titanium (Ti): 3.01%. However, the results confirmed the expected elements (Ba, S, and Ti) in the deposited films. The presence of Si and Ca could result from the substrate composition.

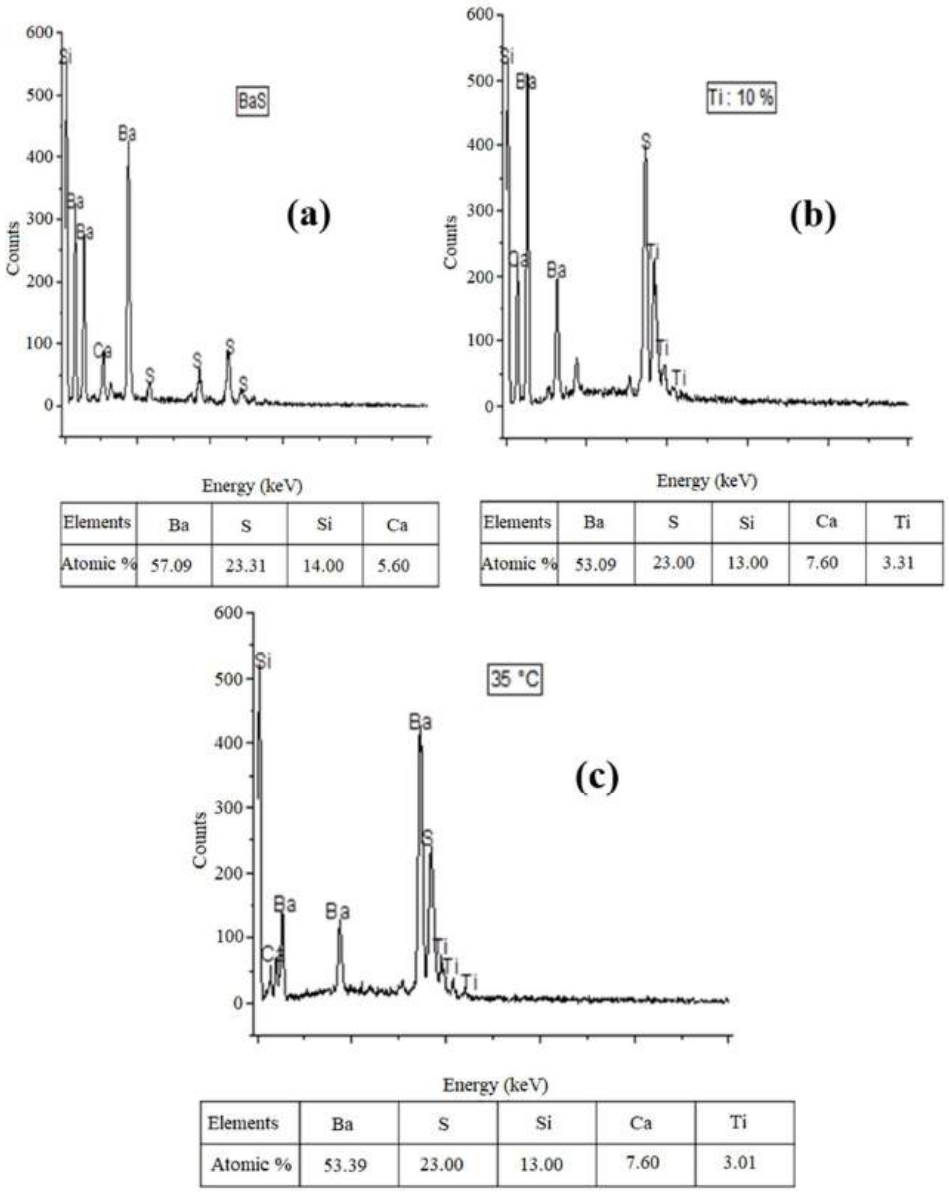

Elements	Ba	S	Si	Ca
Atomic %	57.09	23.31	14.00	5.60

Elements	Ba	S	Si	Ca	Ti
Atomic %	53.09	23.00	13.00	7.60	3.31

Elements	Ba	S	Si	Ca	Ti
Atomic %	53.39	23.00	13.00	7.60	3.01

Fig. 4 (a) EDS graph of the electro-deposited BaS thin film, (b) EDS graph of electro-deposited Ti-doped BaS thin film, and (c), EDS graph of Ti-doped BaS thin film deposited at above room temperature.

D. Effect of deposition temperature on the electrical properties of titanium-doped barium sulfide thin films

Table II displays the Electrical features of barium sulfide thin films doped with titanium, deposited at various temperatures. The obtained result showed that variation in deposition temperature has a significant effect on the electrical properties of the deposited films. As the deposition temperature was increased, the films' electrical resistivity values decreased, while the electrical conductivity increased. Electrical resistivity values that decreased from $11.20 \times 10^{-5}\,\Omega m$ to $1.07 \times 10^{-5}\,\Omega m$, and electrical conductivity values that increased from $8.93 \times 10^{3}\,S/m$ to $93.46 \times 10^{3}\,S/m$, were obtained for the films deposited at temperature 35 °C, 45 °C, and 55 °C, respectively. Fig. 5 depicts the electrical resistivity and conductivity with temperature.

Table II. Electrical characteristics of barium sulfide thin films doped with titanium at varying deposition temperatures.

Temperature (°C)	V $(\times 10^{-3})$ (V)	I $(\times 10^{-4})$ (A)	Thickness (nm)	ρ $(\times 10^{-5})$ $(\Omega\, m)$	$\sigma_e(\times 10^{3})$ (S/m)
35	41.95	2.14	126.10	11.20	8.93
45	31.79	8.51	129.24	2.19	45.66
55	59.83	35.23	139.21	1.07	93.46

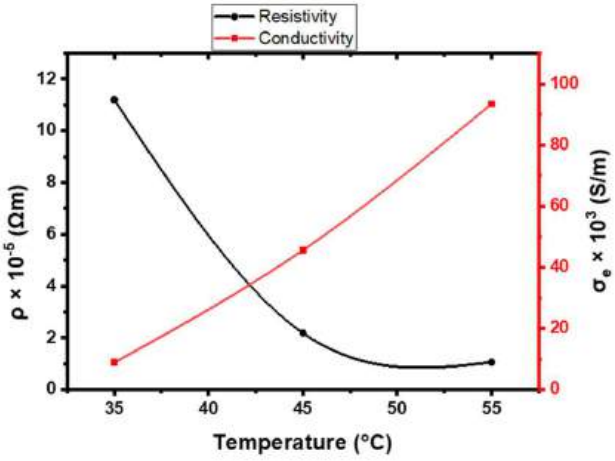

Fig. 5 Variation in electrical resistivity and conductivity with temperature.

E. Effect of temperature on Ti-doped barium sulfide films.

Fig. 6 (a) depicts the graph of absorbance Vs wavelength for titanium-doped copper sulfide thin films electro-deposited at different bath temperatures. A consistent decrease in absorbance was observed across the spectrum as the wavelength of photons increased (from 300 to 1100 nm). The optical absorbance values for the films decreased as the temperature increased: 0.36 to 0.12, 0.43 to 0.17, 0.56 to 0.22, 0.74 to 0.24, and 0.80 to 0.45. The results indicated that the optical absorption values of the films grew as the bath temperature rose. Higher bath temperatures promote the formation of larger and more ordered crystal structures within the films. These well-defined crystals exhibit stronger interactions with light, leading to increased absorption. Elevated temperatures introduce more defects into the film structure. These defects act as additional sites for light absorption, contributing to the overall increase in absorption values. The bandgap energy of a material determines the energy required for electrons to jump from the valence band to the conduction band. Higher bath temperatures influence the bandgap energy, potentially leading to increased absorption in specific wavelength ranges [19], [43]. The absorbance characteristics of the deposited films were satisfactory. It has the potential to be used as an engineering material for antireflective coating. Fig. 6 (b) shows the graph of the transmittance of titanium-doped barium sulfide films deposited at different temperatures Vs wavelengths.

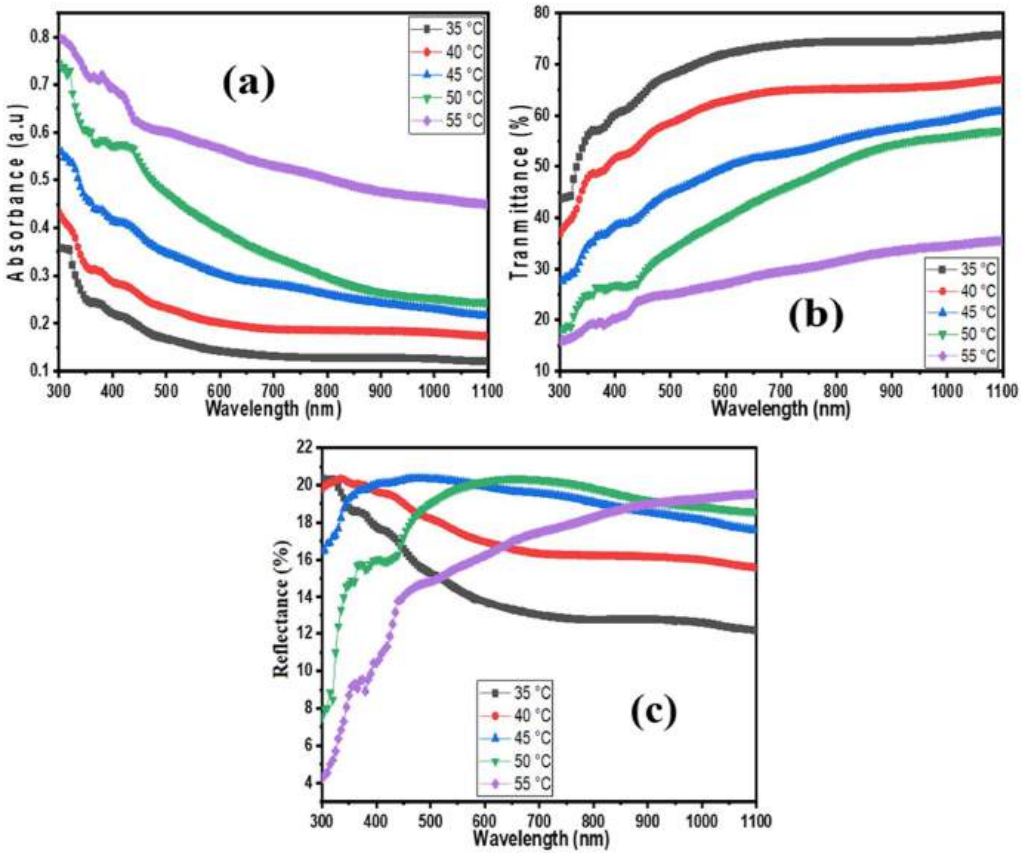

Fig. 6 Plot of absorbance (a), transmittance (b), and reflectance (c) against wavelength for titanium-doped barium sulphide films deposited at different temperatures.

The films showed a consistent rise in transmittance values as the wavelength increased (from 300 to 1100 nm). The films' transmittance values increased from 43.78% to 75.76% at 35 °C, from 36.93% to 67.05% at 40 °C, from 27.56% to 60.85% at 45 °C, from 8.01% to 56.94% at 50 °C, and from 15.89% to 35.48% at 55 °C. As the temperature increased, the films' transmittance values decreased, according to the results. Higher temperatures cause increased scattering of light within the film, reducing the amount of light that is transmitted. Temperature changes affect the structure of the film, potentially leading to a decrease in its transmittance. At higher temperatures, the film absorbs more light, reducing the amount that is transmitted [19], [43]. Fig. 6 (c) depicts the graph of reflectance of the films deposited at different bath temperatures Vs wavelength. The data indicated that the deposited thin films exhibited low reflectance values (≤20.34%). Reflectance values of thin films deposited at 35 °C and 40 °C exhibit a gradual decline with increasing wavelength (300 nm to 1100 nm), as shown in the graph. With an increase in wavelength (from 300 nm to 1100 nm), the reflectance values of the film deposited at 55 °C also increased. Reflectance values of films deposited at 45 °C and 50 °C exhibited a pattern of increasing with wavelength in the UV and certain VIS range, and then decreasing in the NIR region. The difference in reflectance value revealed the notable influence of deposition temperature on the optical reflection of the films.

Fig. 7 (a) depicts the graph of the extinction coefficient of titanium-doped barium sulfide thin films Vs wavelength. The extinction coefficient values of film deposited at a temperature of 35 °C increased from 0.16 to 0.19. The film deposited at 40 °C exhibited extinction coefficient values ranging from 0.19 to 0.28. The film deposited at 45 °C has extinction coefficient values that range from 0.24 to 0.34. The film deposited at 50 °C has extinction coefficient values that range from 0.30 to 0.37, and the films deposited at 55 °C have extinction coefficient values that range from 0.32 to 0.65. The results showed that the extinction coefficient increased with an increase in wavelength. The extinction coefficient of the deposited film increased as the bath temperature was raised. The moderate extinction coefficient values indicate these films could be suitable for use as absorber layers in thin-film solar cells and other optoelectronic devices.

Fig. 7 (b) shows the graph of the refractive index of the films deposited at different values of deposition temperature plotted against the wavelength. The graph illustrates that the refractive index of films decreased with increasing wavelength for those deposited at 35°C and 40°C. With films exposed to higher temperatures, the refractive index exhibited an increase in the UV-VIS range and a decrease in the NIR region as the wavelength extended. The films deposited at temperatures of 35 °C, 40 °C, 45 °C, 50 °C, and 55 °C had refractive index values of 2.63, 2.59, 2.34, 1.67, and 1.38, respectively. The obtained values suggest that these films are ideal for antireflective coating.

Fig. 7 (c) is the graph of the optical conductivity of titanium-doped barium sulfide thin films plotted against wavelength. The Fig. shows that the optical conductivity of the electro-deposited thin films decreased with an increase in wavelength. The films deposited at temperature 35 °C, 40 °C, 45 °C, 50 °C, and 55 °C, recorded optical conductivity values that decreased from $4.12 \times 10^{14} s^{-1}$ to $1.08 \times 10^{14}\ s^{-1}$, $4.85 \times 10^{14} s^{-1}$ to $1.70 \times 10^{14}\ s^{-1}$, $5.56 \times 10^{14} s^{-1}$ to $2.19 \times 10^{14}\ s^{-1}$, $5.09 \times 10^{14} s^{-1}$ to $2.45 \times 10^{14}\ s^{-1}$, and $4.35 \times 10^{14} s^{-1}$ to $4.21 \times 10^{14}\ s^{-1}$, respectively. Also, the effects of temperature variation on the electrodeposited thin films showed in the results that, as temperature increased from 35 °C to 45 °C, the optical conductivity increased, and then started decreasing at 50 °C.

Fig. 7 (d) shows the graph of the real dielectric constant of titanium-doped barium sulfide thin films plotted against wavelength. The results showed that the real dielectric constant of the films electrodeposited at lower temperatures (35 °C and 40 °C) decreased with wavelength. While real dielectric constant of the films electrodeposited at higher temperatures (45 °C, 50 °C, and 55 °C) was found to increase within the UV-VIS regions and decrease towards the NIR region. Real dielectric values that ranged from 6.91–4.16, 6.66–5.05, 5.40–5.58, 2.71–5.87, and 1.80–5.19, were obtained for the films deposited at temperature 35 °C, 40 °C, 45 °C, 50 °C, and 55 °C, respectively.

Fig. 7 (e) shows the graph of the imaginary dielectric constant of titanium-doped barium sulfide thin films plotted against wavelength. The graph revealed that the deposited thin films have little variations in their imaginary dielectric constant values, as wavelength was increasing, except for the film deposited at the highest temperature, which exhibited a drastic increase in imaginary dielectric constant, as wavelength was increasing. The values obtained ranged from 0.82 – 0.79, 0.97 – 1.25, 1.11 – 1.61, 1.02 – 1.80, and 0.87 – 3.09, for the films deposited at temperature 35 °C, 40 °C, 45 °C, 50 °C, and 55 °C respectively.

Fig. 8 depicts the plot of $(\alpha hv)^2$ Vs photon energy for titanium-doped barium sulfide thin films. From extrapolation of the straight portion of the graph estimated energy band gap of the films. The graph along the photon energy axis, where $(\alpha hv)^2 = 0$. The energy band gap of 2.98 eV, 2.90 eV, 2.69 eV, 2.68 eV, and 2.30 eV was obtained for the films deposited at temperatures 35 °C, 40 °C, 45 °C, 50 °C, and 55 °C, respectively. The result indicated that the films' energy band gap decreased as the deposition temperature increased. The varied energy bandgap of the films confirmed the effects of deposition temperature on the films.

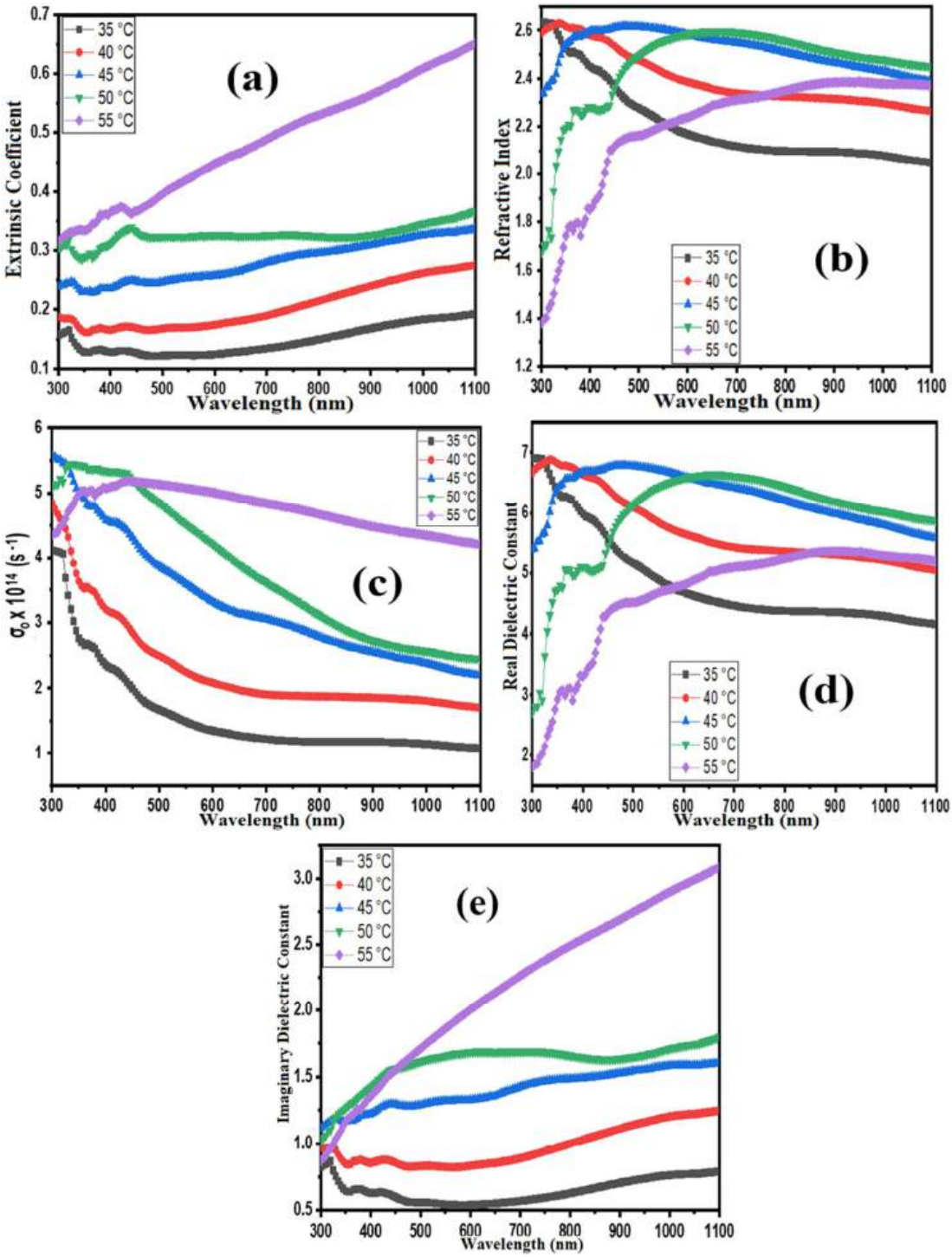

Fig. 7 (a) Extinction coefficient, (b) refractive index, (c) optical conductivity (d) real dielectric constant (e) imaginary dielectric constant against wavelength for titanium-doped barium sulphide films deposited at different temperatures.

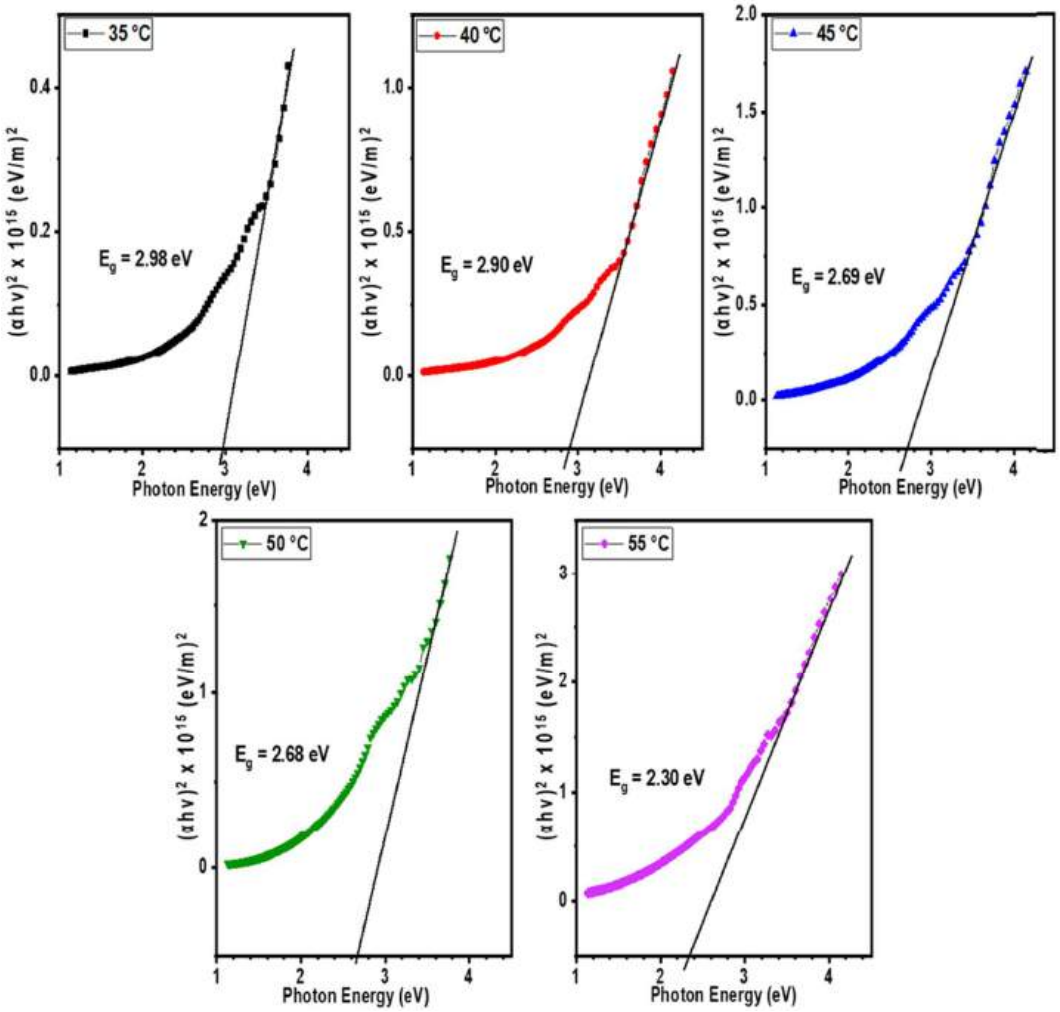

Fig. 8 Plot of $(\alpha hv)^2$ Vs photon energy for titanium-doped barium sulfide films deposited at different temperatures.

IV. Conclusion

BaTiS films have been successfully synthesized using the electrochemical deposition technique. We conducted growth studies on BaTiS films to analyze how the structure was influenced by varying precursor temperatures. The diffraction patterns in the X-ray diffractograms match the cubic barium sulfide structural phase. The observed peaks, 39.994 ° and 65.742 ° at 35 °C; 39.982 ° and 65.717 ° at 45 °C, and 39.995 °, 63.920 °, and 65.856 ° at 55 °C. The film deposited at 55 °C had a surface morphology with uniformly distributed spherical-shaped particles that formed agglomerations. The film's surface was smooth, providing a clearer look at the grain boundaries, suggesting a polycrystalline composition. The films deposited at 35 °C, 40 °C, 45 °C, 50 °C, and 55 °C yielded energy band gaps of 2.98 eV, 2.90 eV, 2.69 eV, 2.68 eV, and 2.30 eV, respectively. The result indicated that the films' energy band gap decreased as the deposition temperature increased. The varied energy bandgap of the films confirmed the effects of deposition temperature on the films.

CREDIT AUTHOR STATEMENT

Emmanuel O. Okechukwu and Imosobomeh L. Ikhioya: conceptualization, methodology, Data curation, Azubuike J. Ekpunobi and Imosobomeh L. Ikhioya: supervisor, data collection, first-draft writing, reviewing, software, and editing. Investigation and visualization. All authors approved the submission.

CONFLICT OF INTEREST

The authors confirm that there are no personal or financial conflicts that may have influenced the study's findings.

AVAILABILITY OF DATA

Data is made freely available on request.

ACKNOWLEDGEMENT

We want to express our gratitude to all the staff of the nano research group at the Department of Physics and Astronomy, University of Nigeria Nsukka for their invaluable assistance, which greatly impacted the research's success.

Reference

[1] I. O. Blessing, H. Shah, S. Afzal, and I. L. Ikhioya, "Enhanced structural properties of electrochemically synthesised NiFeS using 500 keV carbon C++ ions irradiation," Mater. Res. Innov., vol. 00, no. 00, pp. 1–12, 2023, doi: 10.1080/14328917.2023.2262315.

[2] S. O. Malumi,., Malumi, T., Osiele, M. O., Ekpekpo, A., Ikhioya, I. L. 'Enhance and Performance Evolution of Silver-Doped Titanium Dioxide Dye-Sensitized Solar Cells Using Different Dyes', J. of Eng. in Ind. Res., vol. 4, no. 4, pp. 189-200, 2023. doi: 10.48309/jeires.2023.4.1.

[3] A. C. Nkele, I. L. Ikhioya, E. M. Chigozirim, S. O. Aisid, M. Maaza, and F. I. Ezema, "Effects of Erbium on the Properties of Electrochemically-Deposited Zirconium Telluride Thin Films," Nanoarchitectonics, pp. 108–114, 2020, doi: 10.37256/nat.212021503.

[4] A. U. Agobi et al., "Optical and structural properties of graphene oxide-incorporated polyvinylpyrrolidone/copper ternary nanocomposites (PVP/Cu/GO) films," Rev. Mex. Fis., vol. 69, no. 3, pp. 1–9, 2023, doi: 10.31349/RevMexFis.69.031001.

[5] E. O. Ojegu, S. O. Samuel, M. O. Osiele, G. E. Akpojotor, and I. L. Ikhioya, "Optimisation of deposition voltage of zirconium-doped chromium telluride via typical three-electrode cell electrochemical deposition technique," Mater. Res. Innov., vol. 00, no. 00, pp. 1–9, 2023, doi: 10.1080/14328917.2023.2243063.

[6] E. O Ojegu., O. B Odia., Mike O. Osiele M. O., Godfrey A. E., Ikhioya I. L. "Effect of precursor temperature on electrochemically deposited zirconium doped chromium telluride using a standard three-electrode system", J. Mater. Environ. Sci., vol. 14, no. 11, pp. 1148-1159, 2023.

[7] S. G. Sarwar, I. L. Ikhioya, S. Afzal, and I. Ahmad, "Supercapitance performance evaluation of MXene/Graphene/NiO composite electrode via in situ precipitation technique," Hybrid Adv., vol. 4, pp. 100105, 2023. doi: 10.1016/j.hybadv.2023.100105.

[8] N. A. Zarkevich, "Journal of Energy and Power Technology," J. Energy Power Technol., pp. 1–12, 2020, doi: 10.21926/jept.2303024.

[9] K. I. Udofia, I. L. Ikhioya, D. N. Okoli, and A. J. Ekpunobi, "Impact of doping on the physical properties of PbSe chalcogenide material for photovoltaic application," Asian J. Nanosci. Mater., vol. 6, no. 2, pp. 135–147, 2023, doi: 10.26655/AJNANOMAT.2023.2.3.

[10] K. I. Udofia, I. L. Ikhioya, D. N. Okoli, and J. Azubike, "Impact of doping on the physical properties of PbSe chalcogenide material for photovoltaic application," Asian J. of Nanosci. & Original Research. vol. 2, pp. 135–147, 2023, doi: 10.26655/AJNANOMAT.2023.2.3.

[11] H. Shah, S. Afzal, M. Usman, K. Shahzad, and I. L. Ikhioya, "Impact of Annealing Temperature on Lanthanum Erbium Telluride (La0.1Er0.2Te0.2) Nanoparticles Synthesized via Hydrothermal Approach," Adv. J. Chem. Sect. A, vol. 6, no. 4, pp. 342–351, 2023, doi: 10.22034/AJCA.2023.407424.1386.

[12] S. Afzal, S. Tehreem, T. Munir, S. G. Sarwar, and I. L. Ikhioya, "Impact of Transition Metal Doped Bismuth Oxide Nanocomposites on the Bandgap Energy for Photoanode Application," J. of Nano & Mater. Sci. Res., vol. 2, no. 1, pp. 104–109, 2023.

[13] E. O. Ojegu and I. L. Ikhioya. "Investigating the Impact of Temperature on MgSe Structural, Optical and Electrical Features to Optimize its Use in Optoelectronics". J. Eng. Ind. Res., vol. 5, no. 1, 16-26, 2024.

[14] E. O. Ojegu and I. L. Ikhioya, "Electrochemically Deposited Iron Sulphide Material by Adjusting the Deposition Time for Photovoltaic Application," Phy. Access, vol. 4, no. 1, 2024.

[15] I. L. Ikhioya et al., "Electrochemical engineering of ZIF-7 electrode using ion beam technology for better supercapacitor performance," J. Energy Storage, vol. 90, 2024. doi: 10.1016/j.est.2024.111833.

[16] I. Okeoghene Blessing, H. Shah, S. Afzal, and I. L. Ikhioya, "Enhanced structural properties of electrochemically synthesised NiFeS using 500 keV carbon C++ ions irradiation," Mater. Res. Innov., 2023, doi: 10.1080/14328917.2023.2262315.

[17] I. Rufus and I. L. Ikhioya, "Enhanced electrical, morphology, structural, and optical features of nickel silver sulphide material," J. of Basic Phy. Res., vol. 11, no.2, pp. 1- 9, 2023.

[18] A. Hussain, F. Ali, and H. Hammad. "Enhanced specific capacitance, structural, optical, and morphological study of carbon ions incorporated into the lattice of $ZrCuO_2$ nanoparticle synthesized by hydrothermal method," Hybrid Adv., vol. 5, no. January, pp. 100170, 2024, doi: 10.1016/j.hybadv.2024.100170.

[19] I. L. Ikhioya and A. C. Nkele, "Green synthesis and characterization of aluminium oxide nanoparticle using neem leaf extract (Azadirachta Indica)," Hybrid Adv., vol. 5, no. November 2023, pp. 100141, 2024, doi: 10.1016/j.hybadv.2024.100141.

[20] M. A. Mohamed, N. Inami, E. Shikoh, Y. Yamamoto, H. Hori, and A. Fujiwara, "Fabrication of spintronics device by direct synthesis of single-walled carbon nanotubes from ferromagnetic electrodes," Sci. Tech. Adv. Mater., vol. 9, no. 2, 2008, doi: 10.1088/1468-6996/9/2/025019.

[21] Y. Wang, H. Masuda, N. Sato, K. Yamada, And T. Fujino, “Synthesis of BaxTiSy in Sulfur Melt.,” Shigen-to-Sozai, vol. 115, no. 7. pp. 547–552, 1999. doi: 10.2473/shigentosozai.115.547.

[22] D. Aldakov, A. Lefrançois, and P. Reiss, “Ternary and quaternary metal chalcogenide nanocrystals: Synthesis, properties and applications,” J. Mater. Chem. C, vol. 1, no. 24, pp. 3756–3776, 2013, doi: 10.1039/c3tc30273c.

[23] M. M. Alkhamisi, A. F. Qasrawi, and H. K. Khanfar, “Growth and Characterization of Lanthanum Germanide Thin Films by the Thermal Evaporation Technique,” Cryst. Res. Technol., vol. 2300049, pp. 1–8, 2023, doi: 10.1002/crat.202300049.

[24] S. Althobaiti, M. Alghamdi, B. Alamri, and A. Madani, "Structural and optical investigations of Nd and Cu doped BaTiO3 prepared by solid-state reaction," Optik (Stuttg)., vol. 275, 2023, doi: 10.1016/j.ijleo.2023.170534.

[25] E. Bainglass and M. N. Huda, “ Electronic Properties of SbTa 1- x Nb x O 4 : Phase-Related Distortions," J. Electrochem. Soc., vol. 166, no. 5, pp. H3195–H3201, 2019, doi: 10.1149/2.0281905jes.

[26] S. P. Berglund, F. F. Abdi, P. Bogdanoff, A. Chemseddine, D. Friedrich, and R. Van De Krol, “Comprehensive Evaluation of CuBi2O4 as a Photocathode Material for Photoelectrochemical Water Splitting,” Chem. Mater., vol. 28, no. 12, pp. 4231–4242, 2016, doi: 10.1021/acs.chemmater.6b00830.

[27] N. Chaglabou, “Comparative study of the properties of the Cu-M-O thin films (M=In and Sb),” IJERT vol. 2, no. 11, pp. 4195–4201, 2013.

[28] P. Chongngam, E. Wongrat, and A. Tubtimtae, “Optik Effect of annealing temperatures on the structural, optical, and electrical properties of Cu_2Sb thin films,” Optik (Stuttg)., vol. 288, no. July, pp. 171194, 2023, doi: 10.1016/j.ijleo.2023.171194.

[29] I. M. El Radaf, M. S. AlKhalifah, and M. S. El-Bana, “Highlights on the structural, optical, and optoelectrical properties of novel InSbO3 thin films synthesized by chemical bath deposition,” J. Non. Cryst. Solids, vol. 588, no. December 2021, pp. 121612, 2022, doi: 10.1016/j.jnoncrysol.2022.121612.

[30] F. Z. Krimech and S. Sayouri, "Structure and dielectric behaviour of Cu-doped BaTiO3 ceramics," Mater. Today, Proc., vol. 30, pp. 909–917, 2019, doi: 10.1016/j.matpr.2020.04.349.

[31] J. M. Mosby and A. L. Prieto, “Direct electrodeposition of Cu2Sb for lithium-ion battery anodes,” J. Am. Chem. Soc., vol. 130, no. 32, pp. 10656–10661, 2008, doi: 10.1021/ja801745n.

[32] P. B. Patil et al., "Single-step hydrothermal synthesis of hierarchical TiO_2 microflowers with radially assembled nanorods for enhanced photovoltaic performance,” RSC Adv., vol. 4, no. 88, pp. 47278–47286, 2014, doi: 10.1039/c4ra07682f.

[33] S. Pawar and H. Deshmukh, “Hydrothermal method for Synthesis of different Nanostructure Metal Oxide thin film,” Int. J. Innov. Knowl. Concepts, vol. 6, no. February 2020, pp. 126–129, 2018, doi: 11.25835/IJIK-321.

[34] A. J. Perez et al., “Ordered Oxygen Vacancies in the Lithium-Rich Oxide Li4CuSbO5.5, a Triclinic Structure Type Derived from the Cubic Rocksalt Structure,” Inorg. Chem., vol. 60, no. 24, pp. 19022–19034, 2021, doi: 10.1021/acs.inorgchem.1c02882.

[35] A. Rabhi, M. Kanzari, and B. Rezig, “Optical and structural properties of CuSbS2 thin films grown by thermal evaporation method,” Thin Solid Films, vol. 517, no. 7, pp. 2477–2480, 2009, doi: 10.1016/j.tsf.2008.11.021.

[36] G. Y. Senguler, E. K. Narin, S. B. Lisesivdin, and T. Serin, “Effect of sulfur concentration on structural, optical and electrical properties of Cu2CoSnS4 absorber film for photovoltaic devices,” Phys. B Conden. Matter, vol. 648, no. September 2022, p. 414424, 2023, doi: 10.1016/j.physb.2022.414424.

[37] R. G. Sotelo Marquina et al., “CuSbS2 thin films by heat treatment of thermally evaporated Sb_2S_3/CuS stack: Effect of [Cu]/[Sb] ratio on the physical properties of the films,” Vacuum, vol. 204, 2022, doi: 10.1016/j.vacuum.2022.111355.

[38] S. Y. Tee et al., “Thermoelectric Silver-Based Chalcogenides,” Adv. Sci., vol. 9, no. 36, 2022, doi: 10.1002/advs.202204624.

[39] N. A. Okereke and A. J. Ekpunobi, “Chemical bath deposited barium selenide films-structural and optical properties,” Chalcogenide Lett., vol. 8, no. 1, pp. 9–14, 2011.

[40] H. Soonmin, “Deposition of metal sulphide thin films by chemical bath deposition technique: Review,” Int. J. Thin Film Sci. Technol., vol. 10, no. 1, pp. 45–57, 2021, doi: 10.18576/ijtfst/100108.

[41] N. Ijeoma, “Effect Of Film Thickness On The Transmittance Of Chemical Bath Deposited Barium Sulphide ({BaS}) Thin Film,” IJIRAS, vol. 4, no. 2, pp. 3, 2017.

[42] O. D. Nnanyere, “Optical Properties of Barium Sulphide Thin Films Prepared By Chemical Bath Deposition Technique,” IOSR J. App. Phys., vol. 7, no. 4, pp. 10–15, 2015, doi: 10.9790/4861-07421015.

[43] I. L. Ikhioya et al., “Electrochemical engineering of ZIF-7 electrode using ion beam technology for better supercapacitor performance,” J. Energy Storage, vol. 90, no. PA, pp. 111833, 2024, doi: 10.1016/j.est.2024.111833.